Dynamic magnetic hysteresis in single-domain particles with uniaxial anisotropy

I. S. Poperechny, Yu. L. Raikher, and V. I. Stepanov
Institute of Continuous Media Mechanics, Ural Branch, Russian Academy of Sciences, Perm 614013, Russia
(Received 16 August 2010; revised manuscript received 15 October 2010; published 17 November 2010)

On the basis of Brown's kinetic equation a consistent study of the regimes of cyclic magnetization reversal of single-domain particles with a uniaxial anisotropy is performed. The applied field is harmonic and linearly polarized, its amplitude equals the maximal coercive force of a Stoner-Wohlfarth particle. The dynamic magnetic hysteresis loops are obtained for a particle (oriented particle ensemble), whose easy-magnetization axis is tilted to the field direction under an arbitrary angle. It is shown that the Stoner-Wohlfarth regime (often termed as quasistatic) is able to describe the behavior of a nanoparticle only in a quite limited material and external parameter range. The developed approach has at least two major merits: it enables one to consider dynamic magnetic hysteresis in the temperature-frequency domains inaccessible with the aid of approximate methods, and provides a tool to test the accuracy of the latter.

DOI: 10.1103/PhysRevB.82.174423 PACS number(s): 75.75.Jn, 75.60.Ej

I. INTRODUCTION

Magnetic hysteresis in single-domain particles is one of the most interesting effects in the applied physics of magnetic phenomena. At least two important technological areas are entirely based on it. The first is magnetic information storage, where the quality and the lifetime of a record crucially depend on the parameters of the $M(H)$ loop. Another, also very important issue, which requires a detailed knowledge of the magnetization reversal mechanism, is the magnetoinductive hyperthermia. The latter is rapidly progressing in medical science and clinical practice. The above-mentioned subjects, however significant they are, by no means exhaust the variety of applications of magnetically switchable fine particles and of the thermal effect produced with their aid. Meanwhile, until now the theory of hysteresis in single-domain particles has not achieved full clarity. This concerns even the basic problem: magnetization reversal of an isolated particle, let alone the problems of magnetic switching of the particles in ensembles with dipole-dipole interactions.

The first quantitative model of the effect was proposed by Stoner and Wohlfarth.[1] There, to find the equilibrium orientation of the particle magnetic moment, minimization of the internal energy was used. It had turned out soon, that this model, being quite clear and concise at zero temperature, does not have a simple extension for finite-temperature cases. The same relates to finite frequencies despite that in Stoner-Wohlfarth (SW) model the frequency is, formally, arbitrary.

Remarkably, the publication of Ref. 1 almost coincided in time with the prediction[2] and experimental discovery[3] of superparamagnetism, the mechanism that establishes a strong dependence of the nanoparticle remagnetization regimes on temperature, field amplitude, and frequency. Therefore, about 60 years ago, together with the birth of SW and superparamagnetic approaches, there turned up the necessity to understand their interrelation.

The attempts to build up a universally applicable model of magnetic response of a single-domain particle to a strong magnetic field are developing now along two main lines. The first substitutes the energy considerations[1] by some relations from equilibrium statistical thermodynamics.[4,5] In these works the exact angular localization (trajectory) of the particle magnetic moment $\boldsymbol{\mu}$ is replaced by some "orientational smear" of thermal origin, and at a given temperature the obtained set of states is averaged over the Boltzmann distribution. The other line of studies is based on the description of the remagnetization process in terms of a master or Fokker-Planck equation originally derived by Brown.[6] In order to obviate a full statement of the problem that is rather complicated, certain strong simplifications are used,[7–9] all of which are some variations in the Kramers approximation and thus imply that the ratio of the anisotropy energy to thermal one is high.

The first paper, where the kinetic equation was solved in full, dates back to 1974.[10] There, the magnetization reversal in a single-domain particle was considered assuming arbitrary values of the three major parameters, viz., temperature and the amplitude and frequency of the field. However, in Ref. 10 the magnetodynamics of the system was severely simplified: the particle was assumed to be magnetically isotropic, i.e., conventional superparamagnetism was excluded. Due to that, in the absence of an external field the particle magnetic moment is completely degenerated with respect to orientation, thus making impossible a direct comparison of the results of Ref. 10 with those of the SW model. Such rather an unrealistic assumption of Ref. 10 notwithstanding, this paper until now remains very valuable from methodological viewpoint.

A consistent kinetic study of the magnetization dynamics of a single-domain particle with a finite uniaxial anisotropy we began in Refs. 11 and 12, where the case of magnetic field $\boldsymbol{H}$ parallel to the easy-magnetization axis (denoted by a unit vector $\boldsymbol{n}$) was considered. It was shown that for the field with amplitude $H=H_A$ [for the definition of H_A see Eq. (3) below] and moderate frequencies, the dynamic magnetization curves $\mu(H)$ tend to the rectangular loop predicted by the SW model. This evolution is controlled by the "superparamagnetic" parameter E_A/k_BT that is the ratio of the particle anisotropy energy barrier height E_A to thermal energy. In Ref. 11 the dependence of the dynamic magnetic hysteresis (DMH) loops and the energy of an ac field absorbed by

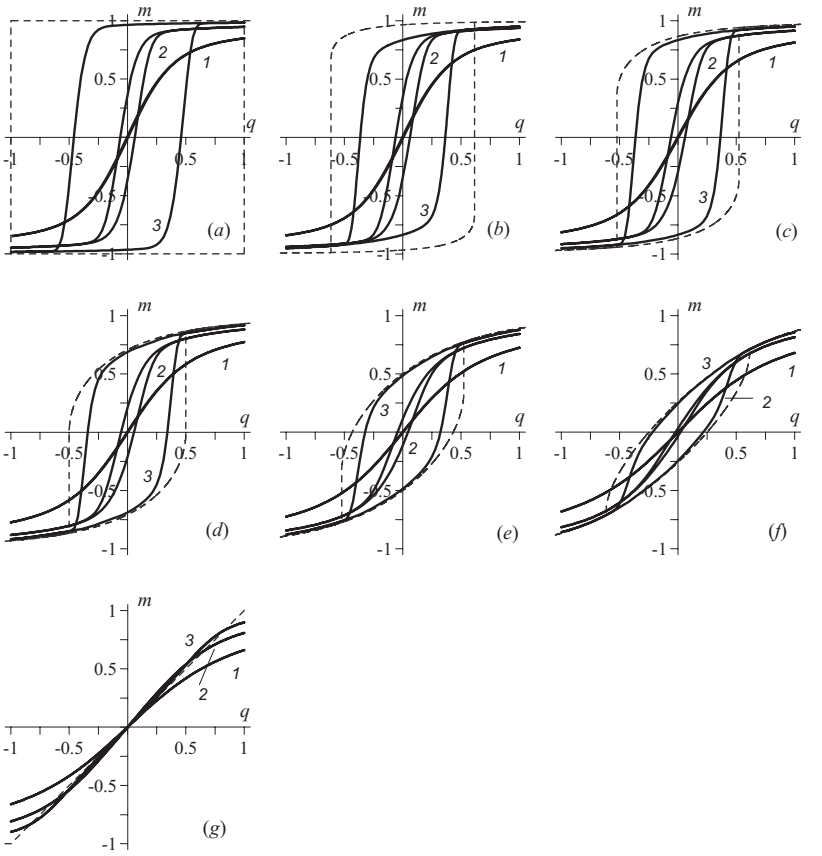

FIG. 1. DMH loops for the tilt angles (a) $\psi=0$, (b) 15°, (c) 30°, (d) 45°, (e) 60°, (f) 75°, and (g) 90°; $\omega\tau_0=10^{-3}$; the anisotropy parameter $\sigma=2$ (line 1), 5 (2) and 15 (3); dashed lines show the respective SW contours.

the particle on the field amplitude H_0 were also considered. The dynamic coercive force as a function of H_0, ω, and T was investigated in Ref. 12.

In what follows a solution of the cyclic magnetization problem for a single-domain particle, whose anisotropy axis is tilted under an arbitrary angle with respect to the linearly polarized field, is given. The sets of loops for various combinations of the particle material parameters, field amplitude, and frequency are presented for orientationally textured and randomly oriented ensembles of noninteracting particles. Our consideration is essentially based on the superparamagnetic theory, i.e., on the Brown's Eq. (4), see below. The solution of this equation—the distribution function W—when expanded in a series of spherical harmonics, yields a countable spectrum of relaxation times. Any observable physical quantity (e.g., the particle magnetic moment) is obtained by averaging a respective dynamic variable with the distribution function W so that the obtained kinetics incorporates the effect of all the infinite relaxation spectrum.

We remark that the DMH cycles shown below in Figs. 1–5 are evaluated in result of calculations, where several tens of the spherical harmonic amplitudes are taken into account and the calculation errors are strictly controlled. As such, these curves are quantitatively correct. However, to make their analysis comprehensible, we use a qualitative approach based on a hypothesis of a single (effective) relaxation time. This enables one to reveal some important features of the DMH process without excessive complications. On the other hand, such a model is quite rough even if to let alone the restricted applicability of the relaxation time concept to nonlinear regimes. So, it is no surprise that certain details of the obtained curves could not be interpreted in this simple framework.

II. KINETIC EQUATION AND THE REFERENCE TIME SCALE

Consider a uniaxial ferrite or ferromagnet particle, whose size ensures its absolute single-domain state, i.e., is of the order of several nanometers. We denote by v the volume of the particle, M_s its magnetization, E_A its anisotropy energy, and present the orientation-dependent part of the particle energy in the form

$$U = -\mu H(\boldsymbol{eh}) - E_A(\boldsymbol{en})^2, \tag{1}$$

where $\boldsymbol{h}$ is a unit vector of the applied field and $\boldsymbol{e}$ a unit vector of the particle magnetic moment, $\boldsymbol{\mu}=M_s v\boldsymbol{e}$.

In the absence of thermal fluctuations ($T\to 0$ and/or a sufficiently large particle), the magnetodynamics is described by the Landau-Lifshitz equation

$$\frac{d\boldsymbol{e}}{dt} = \frac{\gamma}{\mu}\left(\boldsymbol{e}\times\frac{\partial U}{\partial \boldsymbol{e}}\right) + \frac{\alpha\gamma}{\mu}\left[\boldsymbol{e}\times\left(\boldsymbol{e}\times\frac{\partial U}{\partial \boldsymbol{e}}\right)\right], \tag{2}$$

where γ is the gyromagnetic ratio and α a dimensionless damping parameter. The acting magnetic field

$$\boldsymbol{H}_{\text{eff}} = -\frac{1}{\mu}\frac{\partial U}{\partial \boldsymbol{e}} = H\boldsymbol{h} + H_A(\boldsymbol{en})\boldsymbol{n}, \quad H_A = \frac{2E_A}{\mu} \tag{3}$$

that enters Eq. (2), is a sum of the external field and the contribution from uniaxial anisotropy. From Eqs. (2) and (3)

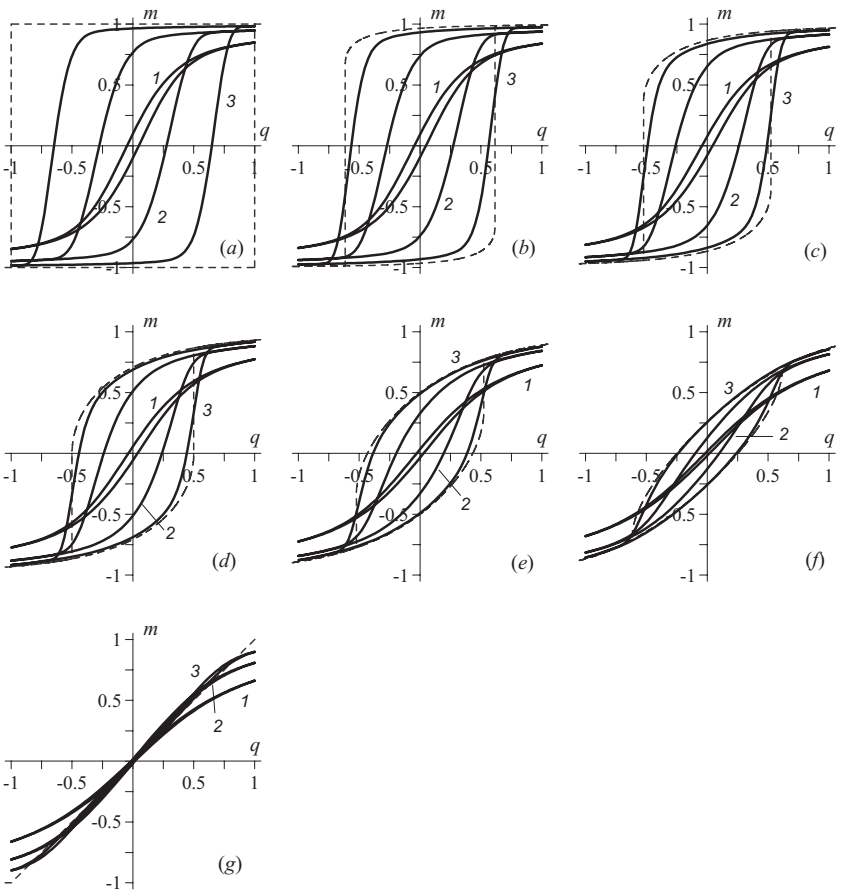

FIG. 2. Same as in Fig. 1 for $\omega\tau_0=10^{-2}$.

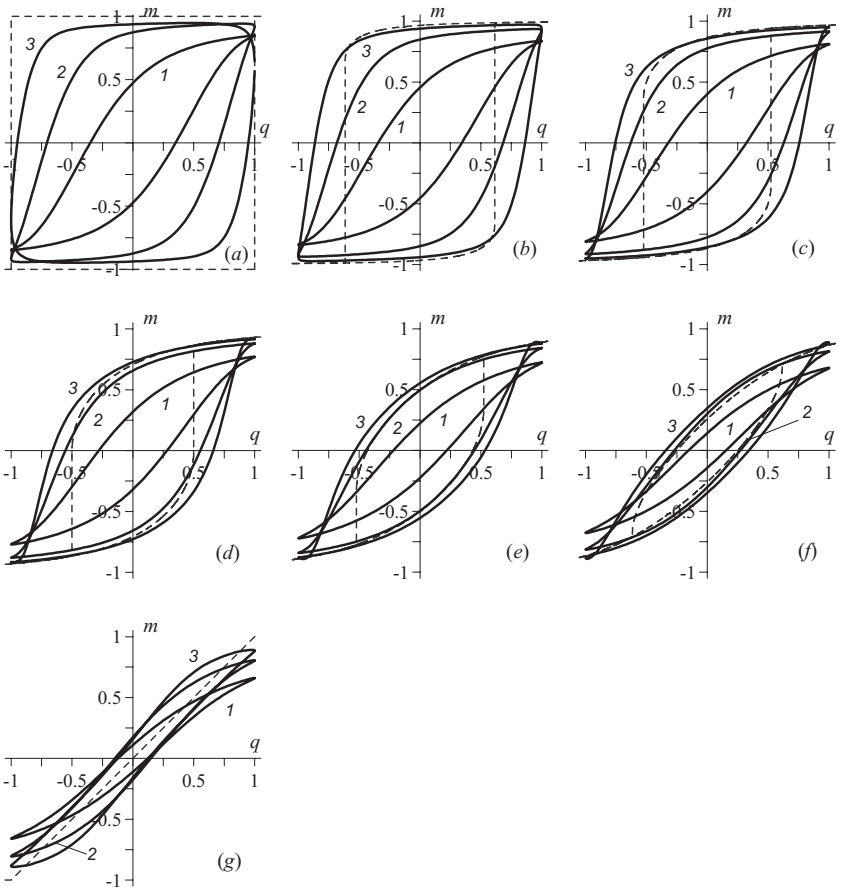

FIG. 3. Same as in Fig. 1 for $\omega\tau_0=10^{-1}$.

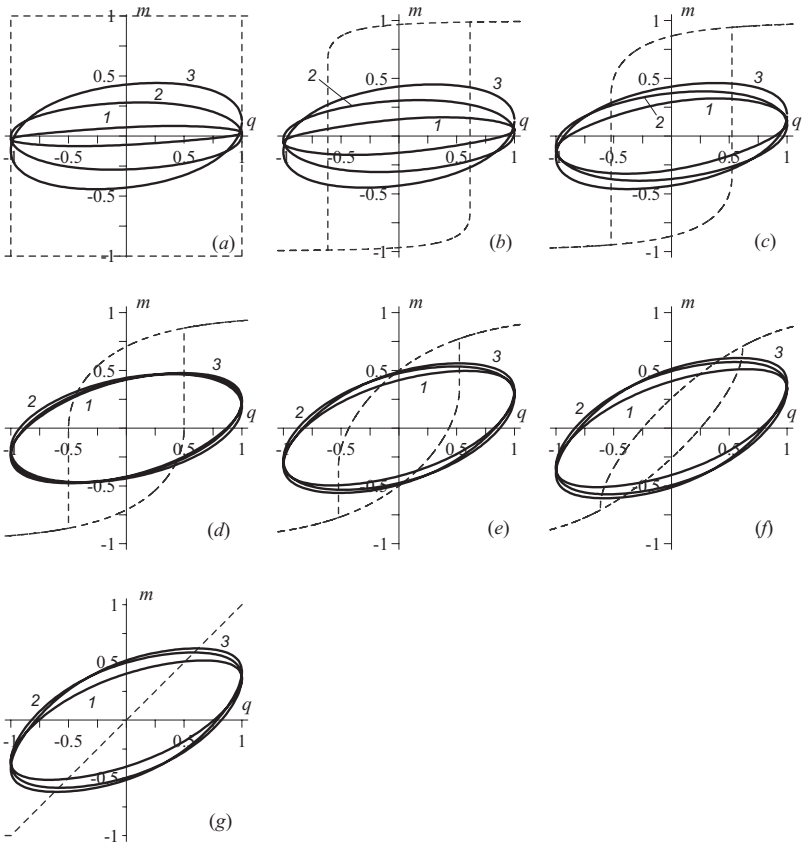

FIG. 4. Same as in Fig. 1 for $\omega\tau_0=1$.

it follows that the magnetic moment proper oscillation is the Larmor precession with the frequency $\omega_L=\gamma H_{\text{eff}}$ and damping time $\tau_L=(\alpha\omega_L)^{-1}$. Under zero external field, the reference relaxation time is determined only by the particle properties, $\tau_0=\mu/2\alpha\gamma E_A$.

In the presence of thermal fluctuations, which induce classical superparamagnetism at $\boldsymbol{H}=0$, the magnetic state of the particle is described by the orientational distribution function $W(\boldsymbol{e},\boldsymbol{H},t)$ that depends parametrically on $\boldsymbol{n}$, and obeys the rotary diffusion (Fokker-Planck) equation[6]

$$2\tau_D\,\partial W/\partial t=\hat{\boldsymbol{J}}W\hat{\boldsymbol{J}}(U/k_BT+\ln W), \tag{4}$$

where $\hat{\boldsymbol{J}}=\boldsymbol{e}\times\partial/\partial\boldsymbol{e}$ is the infinitesimal rotation operator, and $\tau_D=\tau_0E_A/k_BT$ is the reference time of rotary diffusion of the magnetic moment. Under a constant field, Eq. (4) reduces to the condition of static equilibrium, and its solution takes the form of Boltzmann distribution: $W\propto\exp(-U/k_BT)$. Note that the kinetic Eq. (4) does not contain a contribution from the gyration (precession) term of Eq. (3). This means that we restrict further considerations to the limit of so-called intermediate-to-high damping,[13] i.e., assume that parameter α is sufficiently large.

Scaling the magnetic energy terms with thermal energy k_BT, we introduce the dimensionless parameters of the problem

$$\xi=\mu H/k_BT,\quad \sigma=E_A/k_BT,\quad q=\xi/2\sigma=H/H_A. \tag{5}$$

Further on, taking q to be temperature independent, we describe the instantaneous strength of the ac field $H(t)=H_0\cos\omega t$ with the function $q(t)=H(t)/H_A$ of the amplitude $q_0=H_0/H_A$. Assuming that the anisotropy energy E_A is temperature independent, it is convenient to employ the parameter σ introduced in Eq. (5) as the dimensionless inverse temperature, and the product $\omega\tau_0$ as the dimensionless frequency since it does not depend neither on the field nor on temperature. To describe the orientation of the applied field with respect to the particle anisotropy axis, the angle $\psi=\arccos(\boldsymbol{nh})$ is introduced.

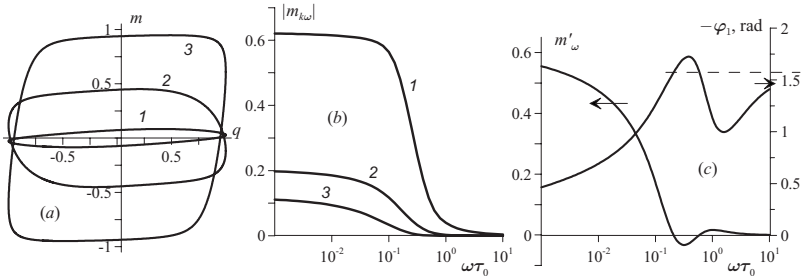

FIG. 5. Panel (a): DMH loops for $\omega\tau_0=0.1$ (1), 0.32 (2), and 1 (3) at $\sigma=15$; panel (b): frequency dependencies of the amplitudes of the first three odd harmonics, i.e., ω, 3ω, and 5ω, of $m(t)$ for $\sigma=15$; panel (c): frequency dependencies of the real part of the first harmonic of $m(t)$ (left) and of its phase lag (right); horizontal line at the left shows the level $\varphi=\pi/2$.

The problem of magnetic relaxation is the key point for all the superparamagnetic theory and for the DMH problem, in particular. The difficulties are mostly due to the fact that the motion of the magnetic moment comprises several time scales. Let us begin with the ground state of the particle ($\boldsymbol{H}=0$) introducing the orientation angle $\theta=\arccos(\boldsymbol{en})$ of vector $\boldsymbol{\mu}$. In this case, potential (1) is bistable: it has two equivalent minima at $\theta=0$ and π separated by a symmetrical barrier of the height E_A centered at $\theta=\pi/2$. If $T=0$, then the magnetic moment is confined in one of the minima, and the particle magnetization reversal, if any, is possible only by the tunnel effect.[14] At a finite but sufficiently low temperature ($\sigma \gtrsim 1$), in the magnetic moment motion two qualitatively different modes could be distinguished. The "fast" (intrawell) mode corresponds to the random walk (diffusion) of vector $\boldsymbol{e}$ about the given potential minimum with the reference time τ_D. The "slow" (interwell) mode corresponds to the fluctuational transitions (flips) of vector $\boldsymbol{e}$ between the minima of the potential $U(\theta)$, i.e., causes the superparamagnetic behavior of a nanoparticle. The reference time of this process $\tau(\sigma,q)$ in the ground state has the order of magnitude $\tau(\sigma,0)\sim\tau_0\exp(\sigma)$ and is widely known as the Néel time. Temperature being diminished (σ grows), the Néel time enhances rapidly. Meanwhile, the intrawell time changes rather weakly and tends to the temperature-independent limit τ_0 at $T\to 0$. On the temperature increase (σ decreases), the difference between the intrawell and interwell times reduces and at $\sigma \ll 1$ virtually disappears since $\tau(\sigma,0)\to\tau_D$.

Let now the external field be nonzero. In this case the orientational potential $U(\theta,\psi)$ looses the symmetry $\theta\leftrightarrow\pi-\theta$, and the positions of its minima are determined by the equation $\boldsymbol{e}\times(\boldsymbol{H}+\boldsymbol{H}_A)=0$. Under not so strong fields, the potential U still has two minima but their depths are different so that one of them is metastable. Accordingly, the times of thermally activated transitions between the minima differ from one another. If the external field exceeds the particle coercive force q_c, one minimum disappears yielding a one-well potential. Given that, the notion of interwell transition is no longer applicable, and the motion of the magnetic moment becomes to much greater extent forced than diffusive. In this limit, the relaxation time does not depend on temperature and decreases unboundedly as the field grows, $\tau(\sigma,q)\sim\tau_H=\tau_D/(\sigma q)=(\alpha\gamma H)^{-1}\propto 1/H$.

In a field with the amplitude $q_0>q_c(\psi)$, that is in the regime where switching is granted, the above-mentioned strong dependence of τ on q entails that during the field cycle the response rate of the magnetic moment changes "on the flight" by orders of magnitude. Due to that, the particle magnetodynamics in a strong ac field could not be reduced to a fixed combination of interwell and intrawell modes; to get a valid description, one has to solve the complete kinetic Eq. (4).

III. SOLUTION OF THE SET OF MOMENT EQUATIONS

Consider Eq. (4) for a mechanically fixed single-domain particle, whose easy-magnetization axis $\boldsymbol{n}$ makes the angle ψ with the direction of a harmonic linearly polarized field $\boldsymbol{H}=H_0\boldsymbol{h}\cos\omega t$ of an arbitrary amplitude. In a spherical frame with the polar axis along $\boldsymbol{n}$, the unit vectors $\boldsymbol{e}$ and $\boldsymbol{h}$ have coordinates $\{\theta,\varphi\}$, $\{0,0\}$, and $\{\psi,0\}$, respectively; then the energy term in the kinetic Eq. (4) takes the form

$$U/k_BT=-\sigma[2q_0\cos\omega t(\cos\psi\cos\theta+\sin\psi\sin\theta\cos\varphi)+\cos^2\theta]. \tag{6}$$

We expand the distribution function in a series

$$W(\theta,\varphi,t)=\sum_{l=0}^{\infty}\sum_{k=-l}^{k=l}b_{l,k}(t)Y_{l,k}(\theta,\varphi) \tag{7}$$

of normalized spherical harmonics defined as

$$Y_{l,k}(\theta,\varphi)=(-1)^k\sqrt{\frac{(2l+1)(l-k)!}{4\pi(l+k)!}}P_l^k(\cos\theta)e^{ik\varphi},\quad -l\le k\le l;\quad Y_{l,k}^*=(-1)^kY_{l,-k}, \tag{8}$$

where P_l^k are associated Legendre polynomials. Coefficients $b_{l,k}$, which determine the time dependence of expansion (7), are the statistical moments of the distribution function

$$b_{l,k}(t)=\int Y^*(\theta,\varphi)W\sin\theta d\theta d\varphi=\langle Y_{l,k}^*(\theta,\varphi)\rangle. \tag{9}$$

Substitution of Eq. (7) in Eq. (4) with allowance for Eq. (6) yields an infinite chain of ordinary differential equations

$$2\tau_0\frac{d}{dt}b_{l,k}+\frac{l(l+1)}{\sigma}b_{l,k}-2\left[\frac{l+1}{2l-1}\sqrt{\frac{(l-k-1)(l+k-1)(l-k)(l+k)}{(2l-3)(2l+1)}}b_{l-2,k}+\frac{l(l+1)-3k^2}{(2l-1)(2l+3)}b_{l,k}\right.$$
$$\left.-\frac{l}{2l+3}\sqrt{\frac{(l-k+2)(l+k+2)(l-k+1)(l+k+1)}{(2l+1)(2l+5)}}b_{l+2,k}\right]-q\cos\psi\left[(l+1)\sqrt{\frac{(l-k)(l+k)}{(2l-1)(2l+1)}}b_{l-1,k}\right.$$
$$\left.-l\sqrt{\frac{(l-k+1)(l+k+1)}{(2l+1)(2l+3)}}b_{l+1,k}\right]-\frac{1}{2}q\sin\psi\left[(l+1)\sqrt{\frac{(l-k-1)(l-k)}{(2l-1)(2l+1)}}b_{l-1,k+1}+l\sqrt{\frac{(l+k+2)(l+k+1)}{(2l+1)(2l+3)}}b_{l+1,k+1}\right.$$
$$\left.-(l+1)\sqrt{\frac{(l+k-1)(l+k)}{(2l-1)(2l+1)}}b_{l-1,k-1}-l\sqrt{\frac{(l-k+2)(l-k+1)}{(2l+1)(2l+3)}}b_{l+1,k-1}\right]=0 \tag{10}$$

with respect to $b_{l,k}$.

After expanding the functions $b_{l,k}(t)$ into a Fourier series with respect to frequency, Eq. (10) yields a set of linear algebraic equations for the three-index coefficients $b^p_{l,k}$. Due to the multidimensionality of the phase space, the derivation of these equations is rather cumbersome; it is given in the Appendix together with the algorithm to obtain a steady solution of this set by matrix sweep method. The latter procedure allows to evaluate the function

$$m(t) = \langle \mathbf{eh} \rangle = \sqrt{\frac{4\pi}{3}}[b_{1,0}(t)\cos\psi - \sqrt{2}b_{1,1}(t)\sin\psi],$$

that is the ensemble average of the projection of the particle magnetic moment on the direction of the field.

IV. DYNAMIC HYSTERESIS: THE RELATION BETWEEN THE KINETIC SCENARIO AND THE STONER-WOHLFARTH APPROXIMATION

Eliminating time as the argument from the pair of functions $m(t)$ and $q(t)$, one arrives at the function $m(q)$ that is a normalized magnetization curve varying within intervals $[-1,1]$ with respect to both m and q. Indeed, as the dimensionless field is defined by Eq. (5), in these units the maximal coercive force of an SW particle equals $q_c(\psi=0) \equiv q_{SW}=1$.

Let us point out the essential difference between the SW and kinetic scenarios of the magnetic hysteresis. In the SW (energy) approach[1] the magnetic moment response time is assumed to be infinitesimal: the switching occurs at this very instant when, under the influence of the applied field, the minimum of the orientational potential, that shelters vector $\boldsymbol{e}$, disappears. The kinetic viewpoint on the process of particle remagnetization is completely different. On the one hand, under a sufficiently slow-changing field the magnetic moment is able to switch from yet existing metastable state. This would happen if the time $\tau(\sigma,q)$ of the thermally activated magnetization reversal, which decreases with the field, would satisfy the condition $\omega\tau(\sigma,q)<1$. On the other hand, at a high frequency, the period of the field might get well below the orientational response time of the magnetic moment, i.e., the relation $\omega\tau(\sigma,q)>1$ would hold even at $q>q_{SW}$. This situation could be termed "kinetic freezing" because, due to its low mobility, the magnetic moment does not depart from its actual orientation despite the fact that with respect to the energy this direction had become utterly unfavorable. In the long run, with the further increase in the field, the condition $\omega\tau(\sigma,q)<1$, i.e., that of "kinetic melting," would eventually occur; however, the value of the field necessary for that could be arbitrarily greater than q_{SW}.

In terms of the kinetic scenario, the magnetization reversal of an SW particle with a given tilt angle ψ is described by the discontinuous conditions

$$\begin{cases} \tau(\sigma,q)=\infty & q<q_{SW} \\ \tau(\sigma,q)=0 & q\geq q_{SW}. \end{cases} \tag{11}$$

which should hold for any nonzero value of the anisotropy parameter σ. Obviously, Eq. (4) does not have solutions compatible with Eq. (11). Therefore, in the framework of kinetic approach, the SW loops are just some benchmark contours, which the magnetization curves tend to in certain particular cases.

The series of Figs. 1–4 gives the details of transformation of $m(q)$ curves obtained by numerical calculations described in Sec. III and Appendix. In these plots the frequency of the field increases from $\omega\tau_0=10^{-3}$ (Fig. 1) to $\omega\tau_0=1$ (Fig. 4), and the field tilt angle varies from $\psi=0°$ to 90°. In each plot we present three curves corresponding to finite temperatures, which we conditionally term high ($\sigma=2$), moderate ($\sigma=5$) and low ($\sigma=15$); by dashes the SW curves (zero temperature, $\sigma=\infty$) are given.

Let us define the effective coercive force q_c as the absolute value of the field q, at which the magnetization turns to zero; the value of q_c depends parametrically on the angle ψ. For an SW particle one has $q_c(\psi)=q_{SW}(\psi)$, and the dependence $q_{SW}(\psi)$ is well known; in particular, $q_c(0)=1$. From the discussion above, it follows that at any finite temperature the DMH loops of a superparamagnetic particle at low frequencies are more narrow than their SW analogs ($q_c<q_{SW}$) while for high frequencies and strong fields they are wider than SW loops ($q_c>q_{SW}$).

The loops would widen until, due to the frequency growth, the condition $\omega\tau(\sigma,1)\ll 1$ that grants switching of the magnetic moment each half period of the field cycle, would be violated. After that, the loops $m(q)$ would shrink along the m axis due to kinetic freezing. From these considerations it also follows that, if at a given value of σ the frequency is increased, then yet greater magnetizing field is necessary to ensure the particle switching. This tendency is easy to retrace comparing Figs. 1–3: one sees that as the parameter $\omega\tau_0$ increases from 10^{-3} to 10^{-1}, the respective loops are wider than the respective SW contours; this happens for all the tilt angles, except for $\psi=0°$ and 90°, see Figs 3(b)–3(f).

V. DYNAMIC HYSTERESIS: TRANSITION TO THE HIGH-FREQUENCY REGIME

The increase in frequency at a given temperature causes the change in magnetodynamic response of the particle: from switching ($\omega\tau_0<1$) to the situation of kinetic freezing ($\omega\tau_0\geq 1$). In the transition region ($\omega\tau_0\lesssim 1$) one encounters a specific phenomenon that qualitatively changes the loop shapes. In Fig. 5(a) curve 2 the loop for $\psi=0$ at $\sigma=15$ (low temperature) and frequency $\omega\tau_0=0.32$ is plotted together with those corresponding to $\omega\tau_0=0.1$ and 1.0. As seen from the figure, the curve 2 is distinguished by the fact that at the field values $|q|\sim 1$ the differential magnetic susceptibility dm/dq becomes negative.

In order to correctly interpret this effect, which might seem anomalous, one has to take into account the following. As is shown in Ref. 15, when proceeding to high frequencies, the magnetic response of a single-domain particle "linearizes": in the frequency spectrum of the magnetization the weights of all the oscillations, except for the first one, fall down rapidly. Therefore, in the range $\omega\tau_0\lesssim 1$ the magnetization comprises just a very little number of harmonics. Our calculation confirms this conclusion. Indeed, from Fig. 5(b), where frequency dependencies of the amplitudes of the first

three harmonics are shown at $\sigma=15$ (low temperature), one sees that in the range $\omega\tau_0 \gtrsim 0.3$ the main part of the magnetization oscillates with the frequency of the field. Let us define the amplitude of the real (in-phase) component of the magnetization $m(q)$ by the relation

$$\mathrm{Re}\, m_\omega \equiv m'_\omega = (\omega/\pi q_0)\int_0^{2\pi/\omega} m(t)q(t)dt. \qquad (12)$$

The frequency dependencies of m'_ω and of the phase lag $|\varphi_1|$ between $m(t)$ and $q(t)$ are presented in Fig. 5(c). As the curves show, in some interval around $\omega\tau_0 \simeq 0.3$ the in-phase part becomes negative and simultaneously $|\varphi_1|$ exceeds $\pi/2$. Clearly, this entails the negativeness of the differential magnetic susceptibility dm/dq and the specific loop shapes like curve 2 in Fig. 5(a).

At the first sight, a smooth line in Fig. 5(c) suggests that there exists a single-valued function $|\varphi|(\omega\tau_0)$, which at a certain frequency surmounts the $\pi/2$ level reminding of the resonance in linear oscillations. In our case, however, the oscillatory motion of the particle magnetic moment is overdamped and completely unable for any resonance. The true origin of both the nonmonotonic behavior of m'_ω and the averaged phase lag shown in Fig. 5(c) is the drastic enhancement of phase fluctuations inside the frequency interval separating the switching and kinetic freezing regimes. Indeed, as the frequency increases, there sooner or later occurs the situation, where the period of the field becomes a bit shorter than the interwell response time. Under this condition, the probabilities for the particle magnetic moment to switch but once during one, two, three, … sequential half periods of the field are comparable. Thence the magnetic moment motion could be looked at as a superposition of regular field-induced weak oscillations and relatively rare random reversals. In result, in correlator Eq. (12) the fraction of states, where the magnetic moment is antiparallel to the field, increases. On the average, this manifests itself as a formal negativeness of m'_ω. With further growth of the frequency, the interwell mode virtually "freezes." Then the phase lag between $m(t)$ and $q(t)$ becomes entirely due to the intrawell relaxation and falls down back to the interval $\varphi < \pi/2$.

Similar effect was discovered before in numeric modeling of the dynamic behavior of multispin systems with thermal noise. A "descend" of the analog of correlator Eq. (12) to the negative region at some frequency interval is described in Ref. 16, where Monte Carlo simulations of DMH in a two-dimensional square-lattice Ising ferromagnet were performed. In Ref. 17 the same behavior of m'_ω was encountered for DMH in plane lattices of elongated iron nanoparticles. From the plot given there (Fig. 1 in Ref. 17) it follows that m'_ω becomes negative in the frequency region that lies in between the switching and linear oscillation regimes. In Ref. 17 the statistical spread of the realizations of m'_ω values was analyzed, and it turned out that in the same interval this spread was anomalously high.

We surmise that the above-mentioned peculiar magnetic behavior is quite universal and is entirely due to the presence of thermal noise. This is supported by the fact that the magnetic structures of the compared systems are very different: a Heisenberg multispin ensemble that remagnetizes via multiple domain nucleation controlled by the nonuniform exchange[16,17] and a considered here absolutely single-domain particle (a single macrospin), whose only mode of magnetization reversal is the coherent rotation.

VI. DYNAMIC HYSTERESIS: HIGH FREQUENCIES

DMH loops at high frequencies ($\omega\tau_0 \geq 1$) are shown in Fig. 4. Here all the curves are quasielliptic, by which they differ strikingly from both the SW and the low-frequency kinetic loops, presented in Figs. 1–3. Evidently, the high-frequency cycles of Fig. 4 have much in common. First, the effective coercive force q_c is close to the maximal attainable value $q_c=1$. Second, the loops rather weakly depend on the angle ψ. Third, for the field inclinations $\psi \gtrsim 45°$ the temperature changes have almost no effect on the loops. Summarizing this, we conclude on universalization of the magnetization process in the high-frequency range.

The following considerations help to understand this situation. At $\omega\tau_0=1$ kinetic freezing is quite strong even at the highest of the considered temperatures ($\sigma=2$). In this limit the Néel (interwell) mode falls out from the relaxation spectrum conceding the dominating role to the fast intrawell modes. This means that the magnetic moment cannot leave a given (initial) potential well, albeit the energy function $U(q,\theta,\psi)$ undergoes dramatic transformations in the course of the field cycle. In other words, an ac field, even of a large amplitude (in our case $q_0=1$) induces only weak oscillations of the magnetic moment about its initial direction. Such a behavior justifies description of the particle magnetodynamics with the aid of linear dynamic susceptibility $\chi(\omega)$. Taking the field in the form $q=q_0 \cos \omega t$ and splitting χ_m into real ($\chi'=m'_\omega/q_0$) and imaginary ($\chi''=m''_\omega/q_0$) parts, one obtains

$$\left(\frac{m-\chi' q}{\chi'' q_0}\right)^2 + \left(\frac{q}{q_0}\right)^2 = 1. \qquad (13)$$

Formula (13) renders a well-known result (see Refs. 9, 11, and 18, for example): a DMH loop of a linearly polarizable particle has an elliptic shape with the major axis tilted under the angle $\delta=\frac{1}{2}\arctan[2\chi'/(1-\chi'^2-\chi''^2)]$. In Ref. 15 the effect of "linearization" of the magnetic response was found only for the case $\psi=0$; our calculations prove, see Fig. 4, that this conclusion holds for any field tilt angle.

The frequency-induced linearization effect suggests that a simple approximation for the high-frequency DMH loops can be obtained from the formulas for the linear dynamic susceptibility of a particle by elimination from them the Néel (interwell) contribution. We present this function as

$$\chi = \chi^{(\perp)} \sin^2 \psi \cdot f_\perp + \chi^{(\parallel)} \cos^2 \psi \cdot f_\parallel, \qquad (14)$$

where $f_{\parallel,\perp}$ are dispersion factors. Valid expressions for the static susceptibility components $\chi^{(\perp)}$ and $\chi^{(\parallel)}$ follow from the results of Ref. 19 and have the form

$$\chi^{(\parallel)} = \left(\frac{1}{2\sigma} + \frac{3}{2\sigma^2} + \frac{25}{4\sigma^3} + \frac{259}{8\sigma^4} + \frac{3177}{16\sigma^5} + \cdots\right), \qquad (15)$$

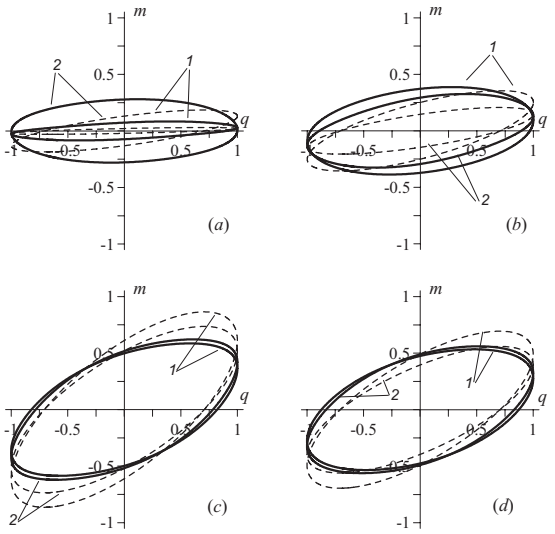

FIG. 6. Comparison of DMH loops, obtained numerically (solid lines) and taken in the dynamic susceptibility approximation, see Eq. (13), for dimensionless temperatures $\sigma=5$ (lines 1) and 15 (*2*) at tilt angles (a) $\psi=0$, (b) 30°, (c) 60°, and (d) 90°; the frequency parameter $\omega\tau_0=1$.

$$\chi^{(\perp)}=\left(1+\frac{1}{2\sigma}+\frac{5}{4\sigma^2}+\frac{37}{8\sigma^3}+\frac{353}{16\sigma^4}+\frac{4081}{32\sigma^5}+\cdots\right). \tag{16}$$

Formulas (15) and (16) correspond to the low-temperature case ($\sigma\gg1$), and in this limit have different temperature behavior. The longitudinal component at $T\to0$ ($\sigma\to\infty$) tends to zero since no moderate field is able to change the magnitude of the particle magnetic moment. Meanwhile, the transverse part in the considered athermic limit remains finite because angular deviations of the magnetic moment from its equilibrium orientation $\boldsymbol{e}\|\boldsymbol{n}$ are always possible. According to relations (14)–(16), a considerable shrinking of the DMH loops under temperature decrease should occur only for $\psi\ll1$. As the angle ψ grows, the fraction of the perpendicular component in the particle response grows, and the temperature dependence of the loops weakens. These qualitative conclusions fairly well agree with the behavior of the numerically obtained plots of Fig. 4.

Assuming that interwell relaxation is absent, we set the dispersion factors in Eq. (14) in the form $f_\perp=f_\parallel=(1+i\omega\tau_0)^{-1}$, thus assuming all the intrawell relaxation times equal. Comparison of approximation formulas (14)–(16) with our numerical results is shown in Fig. 6. A considerable difference is observed only for the angles ψ close to zero. The most probable reason for that is that the form of $f_\parallel$, which we use in formula (14), is oversimplified.

VII. EFFECTIVE COERCIVE FORCE

As follows from Figs. 1–4, by large, the effective coercive force q_c of a nanoparticle grows with temperature diminution (Figs. 1–3), increases with the frequency and goes down when the tilt angle is augmented. The particular dependencies of the coercive force deduced from the numerical calculations are given in Fig. 7. As seen, q_c varies in a wide range and, generally speaking, has little in common with the corresponding SW characteristics. Depending on the particular values of the parameters, the $q_c(\psi)$ curves are located on both sides of the $q_{\mathrm{SW}}(\psi)$ plot and do not have much in common with the latter. Some resemblance could be found only at $\psi\neq0$ in certain angle intervals, see curves 1–3 in Fig. 7(c). This fact once again infers that the predicting force of the SW model is rather limited; we remind that it works only if conditions (11) hold simultaneously.

There are two evident limiting situations for the effective coercive force: the high-temperature and kinetic-freezing regimes. In the first case q_c is very small while in the second it is close to the maximum value. The corresponding transformations could be observed in any of Fig. 7. One sees that, as the frequency increases up to $\omega\tau_0\sim1$, the value of q_c grows logarithmically; meanwhile, the angular dependence of q_c becomes weaker. Beginning with $\omega\tau_0\geq1$, the coercive force (the DMH loop half width) virtually coincides with the field amplitude $q_0=1$. On further increase in frequency, the coercive force at $\psi=0$ does not change but the interval of ψ, where the equality $q_c\approx1$ holds, keeps on widening. To illustrate this tendency, in Fig. 7 a curve for $\omega\tau_0\sim10$ is shown; as seen $q_c\approx1$ practically everywhere.

It does not seem possible to obtain simple closed expressions for q_c under an arbitrary tilt angle. However, an important case of $\psi=0$ is liable for analysis. We do that using a representation for $\tau(\sigma,q)_{\psi=0}$ from Ref. 20. Assuming that the magnetic moment switching occurs at $\omega\tau(\sigma,q)=1$, one finds

$$q_c=1-\sqrt{\frac{1}{\sigma}\ln\left(\frac{1}{\sigma\omega\tau_0}\right)}, \tag{17}$$

provided that condition $\omega\tau_D=\sigma\omega\tau_0<1$ is satisfied. Formula (17) is close kin to a well-known expression[21–23]

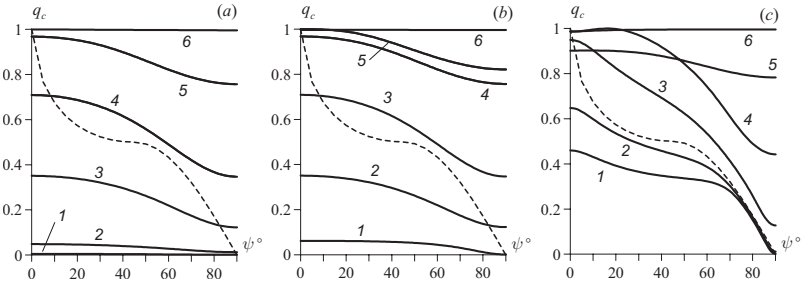

FIG. 7. Angular dependence of the effective DMH coercive force for $q_0=1$; dimensionless temperature (a) $\sigma=2$, (b) 5, and (c) 15; frequency in $\omega\tau_0$ units is 10^{-3} (1), 10^{-2} (2), 0.1 (3), 0.32 (4), 1 (5), and 10 (6); in the scale of figure a curve 1 seem to coincide with the abscissa axis; the dashed line in all the plots corresponds to a SW particle.

$$q_c = 1 - \left[\frac{1}{\sigma}\ln\left(\frac{t_p}{\tau_0}\right)\right]^{1/n}, \tag{18}$$

widely used to deduce the coercive force of nanoparticles from switching field experiments; here t_p is the duration of the field pulse. For the case $\psi=0$ the exponent in Eq. (18) is $n=2$, i.e., coincides with that of Eq. (17). Note that applicability of Eq. (17) to nanoparticles of the type considered here, is restricted to the high-barrier case. For instance, formula (17) agrees well with the numerical calculations for $\omega\tau_0=10^{-3}$ and 10^{-2} at $\sigma=15$ but for the same frequencies and $\sigma=5$ the comparison becomes impossible: Eq. (17) renders negative q_c.

VIII. DISCUSSION

The obtained solutions of the DMH problem cover a wide range of parameters. The studied temperature interval spans from the regime of deep kinetic freezing, i.e., virtual absence of thermally activated magnetization reversal, to the regime of developed superparamagnetism, where thermal motion is the dominating factor. With respect to frequency, the presented model enables one to proceed from virtual equilibrium (single-valued magnetization curve) through the quasistatic (the SW model) and dispersion regimes to the high-frequency limit, where the period of the applied field is shorter that the reference time of spin-lattice relaxation (intrawell) processes. The superparamagnetic effect, due to which the temperature to a great extent affects the particle magnetic relaxation time, causes high temperature-frequency variability of the DMH loops.

The constructed scheme of numerical solution of Brown's equation proved its ability to determine the angular dependencies of DMH in all the above-mentioned regimes. It is found that at a fixed frequency, the influence of the tilt angle on the loop shape is most strong at low temperatures and weakens with the increase in the fluctuation intensity.

In the present work the dependence of DMH on the field amplitude is not investigated, we use all throughout a fixed value $q_0=1$, that is $H_0=H_A$. This choice is usual and follows from a well-known property of the SW model: a field higher than $q_{\mathrm{SW}}=1$ cannot induce any qualitative changes because the magnetization is already saturated. The carried out consideration clarifies the relation between the SW and kinetic models. It turns out that the SW cycles do not belong to the family of regular solutions of the kinetic equation in the sense that they cannot be obtained in result of the limiting transition $T\to 0$. From the general viewpoint, this is due to the fact that the kinetic equation describes the magnetic relaxation to a minimum of the particle free energy, while the SW model, being based on minimization of the particle internal energy, has no time scale inside. Therefore, the SW model is applicable only in the low-temperature range and within the frequency interval whose boundaries (at a given field amplitude) are imposed by the conditions (11).

Only in this temperature-frequency domain the SW loops can indeed play a role of benchmarks with respect to true DMH cycles; Fig. 1 provides an appropriate illustration for that. At any of its plots, the temperature diminution ($\sigma=2$ to $\sigma=15$) brings the DMH curve closer to the respective SW contour (dashed line). However, one should be aware that this tendency is not an ordinary limiting behavior. If to decrease the frequency yet further and to such an extent that the condition $\omega\tau(\sigma,0)\leq 1$ would be attained, the inflation of the loops toward the SW contours would stop and then change for shrinking, ultimately transforming them into single-valued Langevin-type curves characteristic of anhysteretic (equilibrium) magnetization.

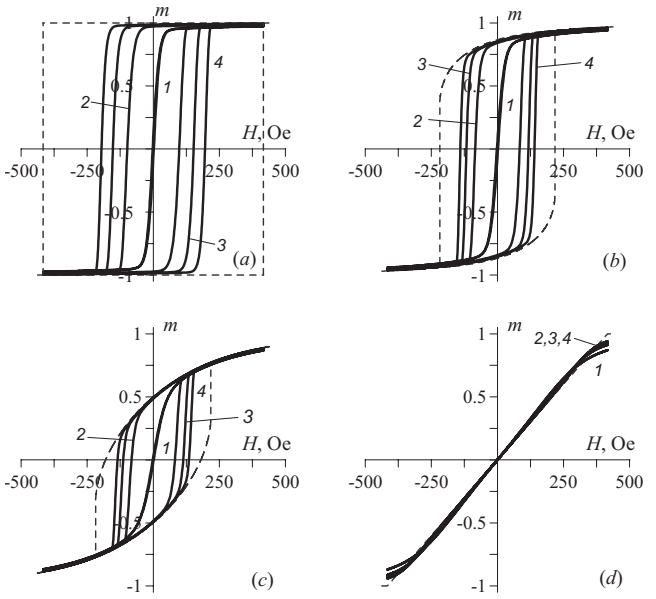

FIG. 8. DMH loops of an ensemble of oriented monodisperse maghemite particles (particle diameter 8 nm, magnetic anisotropy constant 10^5 erg/cm^3) for orientation of the field with respect to the easy axis of the texture (a) $\psi=0$, (b) 30°, (c) 60°, and (d) 90°; plotted curves correspond to temperatures 20 K (1), 10 K (2), 7 K (3), and 5 K (4); dashed lines show the results of the SW model for the same particles and same tilt angles.

An example of how all the found dependencies should manifest themselves in a real system is given in Fig. 8. There we present the DMH loops calculated for an ensemble of noninteracting γ-ferric oxide (maghemite) particles of diameter 8 nm; for their magnetic parameters we set $M_s=480$ G and $E_A=Kv$ with $K=10^5$ erg/cm^3. The considered system is assumed to be orientationally textured, i.e., all the particle easy axes are aligned parallel to one another. The maximal anisotropy field $H_A=2K/M_s$, and, thus, the applied field amplitude, equal 420 G. The frequency parameter in Fig. 8 is $\omega\tau_0=10^{-6}$; with a typical estimation $\tau_0\sim 10^{-10}$ s, this corresponds to dimensional frequency $f\simeq 1$ kHz. Such an amplitude-frequency regime is easily attainable experimentally. As seen from Fig. 8, all the substantial changes in the DMH loops take place in the low-temperature range: $T<20$ K.

When choosing the parameters for the above-given example, we deliberately addressed a case of weakly anisotropic particles because this region is inaccessible with asymptotic methods essentially based on the condition $\sigma\gg 1$. Note that we have encountered limitations imposed by this Kramers-type approach yet in Sec. VII, when it turned out that Eq. (17) is poorly applicable in the parameter do-

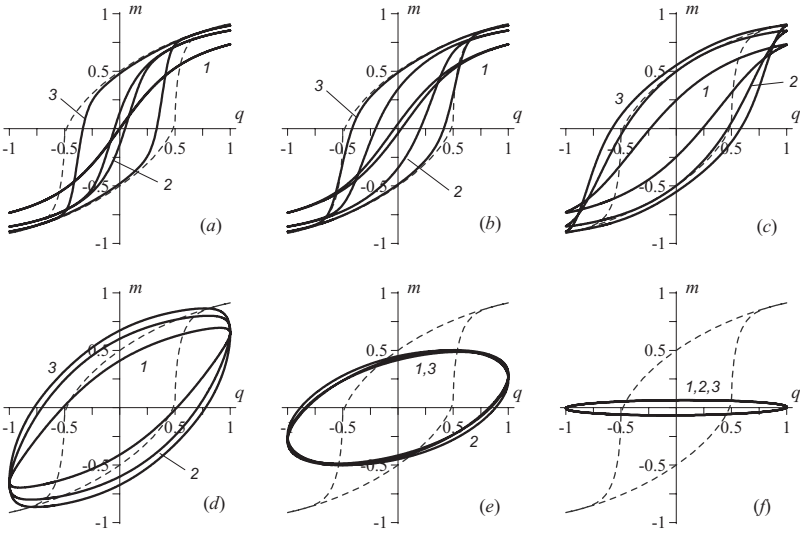

FIG. 9. DMH loops of an ensemble of randomly oriented nanoparticles for frequency parameter (a) $\omega\tau_0=10^{-3}$, (b) 10^{-2}, (c) 0.1, (d) 0.32, (e) 1, and (f) 10; the anisotropy parameter σ (dimensionless inverse temperature) is *2* (line 1), 5 (2), and 15 (3); dashed lines show the result of the SW model for a random particle assembly.

main we deal in. Yet greater errors this approximation would produce when determining the loop shapes, where the dependence of the response time on the instantaneous value of the field strength is a crucial issue. Taking this into account, we infer that our approach, which does not employ any high-barrier approximation, has at least two important merits. First, it enables one to correctly describe DMH in the nanoparticles with weak to moderate anisotropy, and, second, it could be used for ultimate testing of validity of the existing and would-be asymptotic methods.

One more example is given in Fig. 9 where the results of numerical modeling of the frequency- and temperature-induced evolution of DMH loops in an ensemble of particle with randomly oriented easy axes are shown. This distribution seems to be more realistic in comparison with orientationally textured systems. As seen, with the frequency increase the magnetization curves at first approach the SW cycle but after that begin to withdraw from it. The inflation of the loops, see Figs. 9(c) and 9(d), is certainly due to the enhancement of the kinetic freezing effect. Note also that the particles have different tilts of their easy axes, and, hence, they enter the "freezing" regime at different temperatures and frequencies. In result, the loops of Fig. 9 differ considerably from the model loops of textured systems presented in Figs. 1–4. However, qualitatively, the temperature as well as frequency behaviors of the DMH lines follow the same tendencies as those in the oriented ensembles.

IX. CONCLUSIONS

On the basis of Brown's kinetic equation a consistent study of the regimes of cyclic remagnetization (via coherent rotation) of single-domain particles with a uniaxial anisotropy is performed. The applied field is harmonic and linearly polarized, its amplitude equals the maximal coercive force of a Stoner-Wohlfarth particle. The dynamic magnetic hysteresis loops are obtained for a particle (oriented particle ensemble), whose easy-magnetization axis is tilted to the field direction under an arbitrary angle. It is shown that the Stoner-Wohlfarth regime (often termed as quasistatic) is able to describe the behavior of a nanoparticle only in a quite limited material and external parameter range.

Two major limiting cases of the particle magnetic moment behavior—the equilibrium superparamagnetism and kinetic freezing—take place at low and high frequencies, respectively. In the high-frequency range the magnetic response could be described with the aid of a linear dynamic susceptibility. In the frequency scale, the complete kinetic freezing is preceded by the regime, where the statistical average of the phase lag between the magnetic moment and the field exceeds $\pi/2$ and the differential magnetic susceptibility becomes negative. The analysis shows that this effect is inherent to any magnetic system capable of switching and occurs in the situation, where the period of the applied field is close to the reference time scale of the overbarrier magnetic moment fluctuations; in a single-domain particle those fluctuations are responsible for the Néel superparamagnetism.

Our description of the dynamic magnetic hysteresis is valid in a wide field—frequency-temperature domain and is free of oversimplifications such as linear response or high-barrier approximation. This makes it a useful tool for verification of already existing solutions and for studying new problems related to magnetic nanoparticle applications. The most known of the latter is the low-frequency magnetic hyperthermia: heat generation mediated by single-domain particles. Note that the intraparticle dynamic magnetic hysteresis plays the leading role in magnetic heating of both solid and liquid (colloid) nanodisperse systems.[24,25] The processes employed in hyperthermia (under linearly polarized or rotating fields) are steady oscillatory ones. This is exactly the magnetodynamic case that we consider here. Therefore, the results presented here, provided the particle material parameters are specified, can be directly used for theoretical predictions and experiment interpretation.

The developed model is closely related to physics of magnetic recording as well. Apparently, the dynamic magnetic hysteresis could be used to characterize the recording density, signal-to-noise ratio, etc., in a given nanogranular medium. As the effect of thermally driven magnetization reversal (superparamagnetism) is fully accounted for, one would be able to model switching processes for any desirable field-

temperature (thermomagnetic) protocol: heat-assisted or hybrid magnetic recording techniques, for example. The obtained description for the angular dependence of the dynamic magnetic hysteresis (angle ψ in above) could be used to analysis the switching times in the bits of granulated media with allowance for imperfect orientational distributions of the grain easy axes and nonuniformity of the head field inside the recording layer.

ACKNOWLEDGMENTS

The work was done under auspices of RFBR under Project No. 08-02-00802, RFBR-CNRS under Project No. 09-02-91070 (PICS 4825), and ECONET under Project No. 21394NH.

APPENDIX

Let us expand function $b_{l,k}(t)$ in a Fourier series over multiples of the applied field frequency ω and restrict this expansion by a finite number of harmonics,

$$b_{l,k}(t) = \sum_{p=-P}^{p=P} b_{l,k}^{p} e^{ip\omega t}. \tag{A1}$$

Substituting Eq. (A1) in Eq. (10), we get a set of linear algebraic equations for three-index coefficients $b_{l,k}^{p}$

$$\begin{aligned}
&2ip\omega\tau_0 b_{l,k}^{p} + \frac{l(l+1)}{\sigma} b_{l,k}^{p} - 2\left[\frac{l+1}{2l-1}\sqrt{\frac{(l-k-1)(l+k-1)(l-k)(l+k)}{(2l-3)(2l+1)}} b_{l-2,k}^{p} + \frac{l(l+1)-3k^2}{(2l-1)(2l+3)} b_{l,k}^{p}\right. \\
&\left. - \frac{l}{2l+3}\sqrt{\frac{(l-k+2)(l+k+2)(l-k+1)(l+k+1)}{(2l+1)(2l+5)}} b_{l+2,k}^{p}\right] - \frac{1}{2} q_0 \cos\psi\left[(l+1)\sqrt{\frac{(l-k)(l+k)}{(2l-1)(2l+1)}}(b_{l-1,k}^{p-1} + b_{l-1,k}^{p+1})\right. \\
&\left. - l\sqrt{\frac{(l-k+1)(l+k+1)}{(2l+1)(2l+3)}}(b_{l+1,k}^{p-1} + b_{l+1,k}^{p+1})\right] - \frac{1}{4} q_0 \sin\psi\left[(l+1)\sqrt{\frac{(l-k-1)(l-k)}{(2l-1)(2l+1)}}(b_{l-1,k+1}^{p-1} + b_{l-1,k+1}^{p+1})\right. \\
&+ l\sqrt{\frac{(l+k+2)(l+k+1)}{(2l+1)(2l+3)}}(b_{l+1,k+1}^{p-1} + b_{l+1,k+1}^{p+1}) - (l+1)\sqrt{\frac{(l+k-1)(l+k)}{(2l-1)(2l+1)}}(b_{l-1,k-1}^{p-1} + b_{l-1,k-1}^{p+1}) \\
&\left. - l\sqrt{\frac{(l-k+2)(l-k+1)}{(2l+1)(2l+3)}}(b_{l+1,k-1}^{p-1} + b_{l+1,k-1}^{p+1})\right] = 0,
\end{aligned} \tag{A2}$$

for $k \geq 1$. Taking into account the symmetry relation $b_{l,-k} = (-1)^k b_{l,-k}$ that follows from the fact that the statistical moments (9) is real, it is sufficient to solve the set Eq. (A2) for $b_{l,k}^{p}$ with non-negative k's. The equation for $b_{l,0}^{p}$ makes a special case, as its right-hand side contains $b_{l,-1}^{p}$. Expressing the latter coefficient with the aid of the same symmetry rule, one arrives at the equation

$$\begin{aligned}
&2ip\omega\tau_0 b_{l,0}^{p} + \frac{l(l+1)}{\sigma} b_{l,0}^{p} - 2\left[\frac{l(l+1)(l-1)}{(2l-1)}\sqrt{\frac{1}{(2l-3)(2l+1)}} b_{l-2,0}^{p} + \frac{l(l+1)}{(2l-1)(2l+3)} b_{l,0}^{p}\right. \\
&\left. - \frac{l(l+1)(l+2)}{(2l+3)}\sqrt{\frac{1}{(2l+1)(2l+5)}} b_{l+2,0}^{p}\right] - \frac{1}{2} q_0 \cos\psi l(l+1)\left[\sqrt{\frac{1}{(2l-1)(2l+1)}}(b_{l-1,0}^{p-1} + b_{l-1,0}^{p+1})\right. \\
&\left. - \sqrt{\frac{1}{(2l+1)(2l+3)}}(b_{l+1,0}^{p-1} + b_{l+1,0}^{p+1})\right] - \frac{1}{2} q_0 \sin\psi\left[(l+1)\sqrt{\frac{l(l-1)}{(2l-1)(2l+1)}}(b_{l-1,1}^{p-1} + b_{l-1,1}^{p+1})\right. \\
&\left. + l\sqrt{\frac{(l+1)(l+2)}{(2l+1)(2l+3)}}(b_{l+1,0}^{p-1} + b_{l+1,0}^{p+1})\right] = 0.
\end{aligned} \tag{A3}$$

Equations (A2) and (A3) make a closed set that can be presented in the form of a matrix recurrence equation

$$\mathbf{A}_l \boldsymbol{G}_{l-2} + \mathbf{B}_l \boldsymbol{G}_{l-1} + \mathbf{C}_l \boldsymbol{G}_l + \mathbf{D}_l \boldsymbol{G}_{l+1} + \mathbf{E}_l \boldsymbol{G}_{l+2} = 0, \tag{A4}$$

where the following notations are used:

$$\boldsymbol{G}_l = \begin{pmatrix} \boldsymbol{g}_{l,0} \\ \boldsymbol{g}_{l,1} \\ \boldsymbol{g}_{l,2} \\ \cdots \\ \boldsymbol{g}_{l,l-1} \\ \boldsymbol{g}_{l,l} \end{pmatrix}_{(l+1)\times(2P+1)}, \quad \mathbf{A}_l = \begin{pmatrix} \mathbf{a}_{l,0} & \mathbf{0} & \mathbf{0} & \mathbf{0} \\ \mathbf{0} & \mathbf{a}_{l,1} & \mathbf{0} & \mathbf{0} \\ \cdots & \cdots & \cdots & \cdots \\ \mathbf{0} & \mathbf{0} & \mathbf{0} & \mathbf{a}_{l,l} \end{pmatrix}_{(l+1)(2P+1)\times(l-1)(2P+1)},$$

$$\mathbf{B}_l = \begin{pmatrix} \mathbf{v}_{l,0} & \mathbf{v}^+_{l,0} & \mathbf{0} & \mathbf{0} & \mathbf{0} & \cdots & \mathbf{0} & \mathbf{0} & \mathbf{0} & \mathbf{0} \\ \mathbf{v}^-_{l,1} & \mathbf{v}_{l,1} & \mathbf{v}^+_{l,1} & \mathbf{0} & \mathbf{0} & \cdots & \mathbf{0} & \mathbf{0} & \mathbf{0} & \mathbf{0} \\ \mathbf{0} & \mathbf{v}^-_{l,2} & \mathbf{v}_{l,2} & \mathbf{v}^+_{l,2} & \mathbf{0} & \cdots & \mathbf{0} & \mathbf{0} & \mathbf{0} & \mathbf{0} \\ \mathbf{0} & \mathbf{0} & \mathbf{v}^-_{l,3} & \mathbf{v}_{l,3} & \mathbf{v}^+_{l,3} & \cdots & \mathbf{0} & \mathbf{0} & \mathbf{0} & \mathbf{0} \\ \cdots & \cdots & \cdots & \cdots & \cdots & \cdots & \cdots & \cdots & \cdots & \cdots \\ \mathbf{0} & \mathbf{0} & \mathbf{0} & \mathbf{0} & \mathbf{0} & \cdots & \mathbf{0} & \mathbf{v}^-_{l,l-2} & \mathbf{v}_{l,l-2} & \mathbf{v}^+_{l,l-2} \\ \mathbf{0} & \mathbf{0} & \mathbf{0} & \mathbf{0} & \mathbf{0} & \cdots & \mathbf{0} & \mathbf{0} & \mathbf{v}^-_{l,l-1} & \mathbf{v}_{l,l-1} \\ \mathbf{0} & \mathbf{0} & \mathbf{0} & \mathbf{0} & \mathbf{0} & \cdots & \mathbf{0} & \mathbf{0} & \mathbf{0} & \mathbf{v}^-_{l,l} \end{pmatrix}_{(l+1)(2P+1)\times l(2P+1)},$$

$$\mathbf{C}_l = \begin{pmatrix} \mathbf{c}_{l,0} & \mathbf{0} & \cdots & \mathbf{0} \\ \mathbf{0} & \mathbf{c}_{l,1} & \cdots & \mathbf{0} \\ \cdots & \cdots & \cdots & \cdots \\ \mathbf{0} & \mathbf{0} & \cdots & \mathbf{c}_{l,1} \end{pmatrix}_{(l+1)(2P+1)\times(l+2)(2P+1)},$$

$$\mathbf{D}_l = \begin{pmatrix} \mathbf{d}_{l,0} & \mathbf{d}^+_{l,0} & \mathbf{0} & \mathbf{0} & \mathbf{0} & \cdots & \mathbf{0} & \mathbf{0} & \mathbf{0} & \mathbf{0} & \mathbf{0} \\ \mathbf{d}^-_{l,1} & \mathbf{d}_{l,1} & \mathbf{d}^+_{l,1} & \mathbf{0} & \mathbf{0} & \cdots & \mathbf{0} & \mathbf{0} & \mathbf{0} & \mathbf{0} & \mathbf{0} \\ \mathbf{0} & \mathbf{d}^-_{l,2} & \mathbf{d}_{l,2} & \mathbf{d}^+_{l,2} & \mathbf{0} & \cdots & \mathbf{0} & \mathbf{0} & \mathbf{0} & \mathbf{0} & \mathbf{0} \\ \mathbf{0} & \mathbf{0} & \mathbf{d}^-_{l,3} & \mathbf{d}_{l,3} & \mathbf{d}^+_{l,3} & \cdots & \mathbf{0} & \mathbf{0} & \mathbf{0} & \mathbf{0} & \mathbf{0} \\ \cdots & \cdots & \cdots & \cdots & \cdots & \cdots & \cdots & \cdots & \cdots & \cdots & \cdots \\ \mathbf{0} & \mathbf{0} & \mathbf{0} & \mathbf{0} & \mathbf{0} & \cdots & \mathbf{d}^-_{l,l-2} & \mathbf{d}_{l,l-2} & \mathbf{d}^+_{l,l-2} & \mathbf{0} & \mathbf{0} \\ \mathbf{0} & \mathbf{0} & \mathbf{0} & \mathbf{0} & \mathbf{0} & \cdots & \mathbf{0} & \mathbf{d}^-_{l,l-1} & \mathbf{d}_{l,l-1} & \mathbf{d}^+_{l,l-1} & \mathbf{0} \\ \mathbf{0} & \mathbf{0} & \mathbf{0} & \mathbf{0} & \mathbf{0} & \cdots & \mathbf{0} & \mathbf{0} & \mathbf{d}^-_{l,l} & \mathbf{d}_{l,l} & \mathbf{d}^+_{l,l} \end{pmatrix}_{(l+1)(2P+1)\times(l+1)(2P+1)},$$

$$\mathbf{E}_l = \begin{pmatrix} \mathbf{e}_{l,0} & \mathbf{0} & \cdots & \mathbf{0} & \mathbf{0} & \mathbf{0} \\ \mathbf{0} & \mathbf{e}_{l,1} & \cdots & \mathbf{0} & \mathbf{0} & \mathbf{0} \\ \cdots & \cdots & \cdots & \cdots & \cdots & \cdots \\ \mathbf{0} & \mathbf{0} & \cdots & \mathbf{e}_{l,l} & \mathbf{0} & \mathbf{0} \end{pmatrix}_{(l+1)(2P+1)\times(l+3)(2P+1)}.$$

In above and hereafter the subscript indicates the number rows × columns of a matrix.

Vector $\boldsymbol{G}_l$ and matrices $\mathbf{A}_l \ldots \mathbf{E}_l$ are constructed of blocks. Vector $\boldsymbol{G}_l$ could be presented as a set of subvectors $\boldsymbol{g}_{l,k}$ arranged as

$$\boldsymbol{g}_{l,k} = \begin{pmatrix} b^{-P}_{l,k} \\ b^{-P+1}_{l,k} \\ b^{-P+2}_{l,k} \\ \cdots \\ b^{P-1}_{l,k} \\ b^{P}_{l,k} \end{pmatrix}_{2P+1},$$

and matrices $\mathbf{A}_l \ldots \mathbf{E}_l$ consist of square submatrices

$$\mathbf{0} = \begin{pmatrix} 0 & 0 & \cdots & 0 \\ 0 & 0 & \cdots & 0 \\ \cdots & \cdots & \cdots & \cdots \\ 0 & 0 & \cdots & 0 \end{pmatrix}_{(2P+1)\times(2P+1)}, \quad \mathbf{a}_{l,k} = -2\frac{(l+1)}{(2l-1)}\sqrt{\frac{(l-k-1)(l+k-1)(l-k)(l+k)}{(2l-3)(2l+1)}}\mathbf{I}_1,$$

$$\mathbf{v}^{-}_{l,k} = \frac{1}{4}q_0 \sin\psi(l+1)\sqrt{\frac{(l+k-1)(l+k)}{(2l-1)(2l+1)}}\mathbf{I}_2, \quad \mathbf{v}_{l,k} = -\frac{1}{2}q_0 \cos\psi(l+1)\sqrt{\frac{(l-k)(l+k)}{(2l-1)(2l+1)}}\mathbf{I}_2,$$

$$\mathbf{v}^{+}_{l,k\geq 1} = -\frac{1}{4}q_0 \sin\psi(l+1)\sqrt{\frac{(l-k-1)(l-k)}{(2l-1)(2l+1)}}\mathbf{I}_2, \quad \mathbf{v}^{+}_{l,0} = -\frac{1}{2}q_0 \sin\psi(l+1)\sqrt{\frac{l(l-1)}{(2l-1)(2l+1)}}\mathbf{I}_2,$$

$$\mathbf{c}_{l,k} = 2i\omega\tau_0 \begin{pmatrix} -P & 0 & 0 & 0 & 0 & 0 \\ 0 & -P+1 & 0 & 0 & 0 & 0 \\ 0 & 0 & -P+2 & 0 & 0 & 0 \\ \cdots & \cdots & \cdots & \cdots & \cdots & \cdots \\ 0 & 0 & 0 & 0 & P-1 & 0 \\ 0 & 0 & 0 & 0 & 0 & P \end{pmatrix}_{(2P+1)\times(2P+1)} + \left[\frac{l(l+1)}{\sigma} - 2\frac{l(l+1)-3k^2}{(2l-1)(2l+3)}\right]\mathbf{I}_1,$$

$$\mathbf{d}^{-}_{l,k} = \frac{1}{4}q_0 l \sin\psi\sqrt{\frac{(l-k+2)(l-k+1)}{(2l+1)(2l+3)}}\mathbf{I}_2, \quad \mathbf{d}_{l,k} = \frac{1}{2}q_0 l \sin\psi\sqrt{\frac{(l-k+1)(l+k+1)}{(2l+1)(2l+3)}}\mathbf{I}_2,$$

$$\mathbf{d}^{+}_{l,k\geq 1} = -\frac{1}{4}q_0 l \sin\psi\sqrt{\frac{(l+k+2)(l+k+1)}{(2l+1)(2l+3)}}\mathbf{I}_2, \quad \mathbf{d}_{l,0} = -\frac{1}{2}q_0 l \sin\psi\sqrt{\frac{(l+1)(l+2)}{(2l+1)(2l+3)}}\mathbf{I}_2,$$

$$\mathbf{e}_{l,k} = \frac{2l}{2l+3}\sqrt{\frac{(l-k+2)(l+k+2)(l-k+1)(l+k+1)}{(2l+1)(2l+5)}}\mathbf{I}_1,$$

where

$$\mathbf{I}_1 = \begin{pmatrix} 1 & 0 & 0 & \cdots & 0 & 0 \\ 0 & 1 & 0 & \cdots & 0 & 0 \\ 0 & 0 & 1 & \cdots & 0 & 0 \\ \cdots & \cdots & \cdots & \cdots & \cdots & \cdots \\ 0 & 0 & 0 & \cdots & 1 & 0 \\ 0 & 0 & 0 & \cdots & 0 & 1 \end{pmatrix}_{(2P+1)\times(2P+1)}, \quad \mathbf{I}_2 = \begin{pmatrix} 0 & 1 & 0 & \cdots & 0 & 0 & 0 & 0 \\ 1 & 0 & 1 & \cdots & 0 & 0 & 0 & 0 \\ 0 & 1 & 0 & \cdots & 0 & 0 & 0 & 0 \\ \cdots & \cdots & \cdots & \cdots & \cdots & \cdots & \cdots & \cdots \\ 0 & 0 & 0 & \cdots & 1 & 0 & 1 & 0 \\ 0 & 0 & 0 & \cdots & 0 & 1 & 0 & 1 \\ 0 & 0 & 0 & \cdots & 0 & 0 & 1 & 0 \end{pmatrix}_{(2P+1)\times(2P+1)}.$$

Note that the objects $\boldsymbol{g}_{l,k}$ and $\mathbf{a}_{l,k}\ldots\mathbf{e}_{l,k}$ are not the elements of the respective matrices but their minors, i.e., parts.

The set (A4) is solved by matrix sweep method. We denote

$$\boldsymbol{G}_l = \boldsymbol{\alpha}_l\boldsymbol{G}_{l-1} + \boldsymbol{\beta}_l\boldsymbol{G}_{l-2}, \quad \boldsymbol{G}_{l+1} = \boldsymbol{\alpha}_{l+1}\boldsymbol{G}_l + \boldsymbol{\beta}_{l+1}\boldsymbol{G}_{l-1}, \quad \boldsymbol{G}_{l+1} = (\boldsymbol{\alpha}_{l+2}\boldsymbol{\alpha}_{l+1} + \boldsymbol{\beta}_{l+2})\boldsymbol{G}_l + \boldsymbol{\alpha}_{l+2}\boldsymbol{\beta}_{l+1}\boldsymbol{G}_{l-1}. \tag{A5}$$

After substituting Eq. (A5) in Eq. (A4) and comparison with Eq. (A4), one arrives the recurrence equation for the matrix sweeping coefficients

$$\boldsymbol{\alpha}_l = -\boldsymbol{\Delta}^{-1}(\mathbf{B}_l + \mathbf{D}_l\boldsymbol{\beta}_{l+1}\mathbf{E}_l\boldsymbol{\alpha}_{l+2}\boldsymbol{\beta}_{l+1}), \quad \boldsymbol{\beta}_l = -\boldsymbol{\Delta}^{-1}\mathbf{A}_l, \tag{A6}$$

where

$$\boldsymbol{\Delta} = \boldsymbol{C}_l + \boldsymbol{D}_l\boldsymbol{\alpha}_{l+1} + \boldsymbol{E}(\boldsymbol{\alpha}_{l+2}\boldsymbol{\alpha}_{l+1} + \boldsymbol{\beta}_{l+2}).$$

Expansion (A6) is truncated to a finite number L of terms by setting $\boldsymbol{G}_L = \boldsymbol{G}_{L+1} = \ldots = 0$, $\boldsymbol{\alpha}_L = \boldsymbol{\alpha}_{L+1} = \ldots = 0$, $\boldsymbol{\beta}_L = \boldsymbol{\beta}_{L+1} = \ldots = 0$. Using this condition, with the aid of Eq. (A5), we find $\boldsymbol{\alpha}_1$. Then, with allowance for relation $\boldsymbol{G}_0 = \{0,0,\ldots,\frac{1}{\sqrt{4\pi}},\ldots,0,0\}$ following from $b^0_{0,0} = \frac{1}{\sqrt{4\pi}}$ and $b^{k\neq 0}_{0,0} = 0$, we evaluate $\boldsymbol{G}_1$ and finally the dimensionless magnetization $\langle(\boldsymbol{eh})\rangle$.

[1] E. C. Stoner and E. P. Wohlfarth, Proc. R. Soc. London, Ser. A **249**, 599 (1948).
[2] L. Néel, Ann. Geophys. (C.N.R.S.) **5**, 99 (1949).
[3] C. P. Bean and I. S. Jacobs, J. Appl. Phys. **27**, 1448 (1956).
[4] V. Franco and A. Conde, J. Magn. Magn. Mater. **278**, 28 (2004).
[5] C. Tannous and J. Gieraltowski, Physica B **403**, 3578 (2008).
[6] W. F. Brown, Phys. Rev. **130**, 1677 (1963).
[7] J. J. Lu, J. H. Huang, and I. Klik, J. Appl. Phys. **76**, 1726 (1994).
[8] N. A. Usov and Y. V. Grebenshchikov, J. Appl. Phys. **106**, 023917 (2009).
[9] P. Durand and I. Paidarová, EPL **89**, 67004 (2010).
[10] V. A. Ignatchenko and R. S. Gekht, Sov. Phys. JETP **40**, 750 (1975).
[11] Y. L. Raikher, V. I. Stepanov, and R. Perzynski, Physica B **343**, 262 (2004).
[12] Y. L. Raikher and V. I. Stepanov, J. Magn. Magn. Mater. **300**, e311 (2006).
[13] W. T. Coffey, Y. P. Kalmykov, and J. Waldron, *The Langevin Equation*, 2nd ed. (World Scientific, Singapore, 2004).
[14] E. M. Chudnovsky and J. Tejada, *Macroscopic Quantum Tunneling of the Magnetic Moment*, Cambridge Studies in Magnetism (Cambridge University Press, Cambridge, 1998).
[15] P.-M. Déjardin and Y. P. Kalmykov, J. Appl. Phys. **106**, 123908 (2009).
[16] S. W. Sides, P. A. Rikvold, and M. A. Novotny, Phys. Rev. E **57**, 6512 (1998).
[17] G. Brown, M. A. Novotny, and P. A. Rikvold, Physica B **306**, 117 (2001).
[18] R. Skomski, *Simple Models of Magnetism* (Oxford University Press, New York, 2008).
[19] Y. L. Raikher and V. I. Stepanov, Phys. Rev. B **66**, 214406 (2002).
[20] A. Aharoni, Phys. Rev. **177**, 793 (1969).
[21] M. P. Sharrock, J. Appl. Phys. **76**, 6413 (1994).
[22] R. Skomski, J. Phys.: Condens. Matter **15**, R841 (2003).
[23] R. Skomski and D. J. Sellmyer, in *Handbook of Advanced Magnetic Materials*, Nanostructural Effects Vol. 1, edited by Y. I. Liu, D. J. Sellmyer, and D. Shindo (Springer+Media, New York, 2006) Chap. 1, pp. 1–57.
[24] J.-P. Fortin, C. Wilhelm, J. Servais, C. Ménager, J.-C. Bacri, and F. Gazeau, J. Am. Chem. Soc. **129**, 2628 (2007).
[25] E. Duguet, L. Hardel, and S. Vasseur, in *Thermal Nanosystems and Nanomaterials*, Topics in Applied Physics Vol. 118, edited by S. Volz (Springer-Verlag, Berlin, 2009), Chap. 11, pp. 343–365.